Journal of Sound and Vibration (1999) **223**(4), 587–609
Article No. jsvi.1998.2107, available online at http://www.idealibrary.com on IDEAL®

VALIDATION OF A MODEL FOR RAILWAY ROLLING NOISE USING FIELD MEASUREMENTS WITH SINUSOIDALLY PROFILED WHEELS

D. J. THOMPSON
Institute of Sound and Vibration Research, *University of Southampton*, *Highfield*, *Southampton SO*17 1*BJ*, *England*
N. VINCENT
VIBRATEC, 6 *Chemin de l'Industrie - B.P*.69, 69572 *Dardilly Cedex*, *France*
AND
P. E. GAUTIER
SNCF Direction de la Recherche, 45 *rue de Londres*, 75379 *Paris Cedex* 08, *France*

(*Received* 9 *March* 1998, *and in final form* 3 *December* 1998)

Field measurements have been carried out using a series of railway wheels with specially machined running surfaces. These were given a sinusoidal profile around their circumference. This allows accurate measurements of noise and vibration to be made for single frequency excitation. A series of wheels with different wavelengths has been used in combination with a range of running speeds to allow a wide frequency range to be scanned. Results are compared with predictions using a theoretical model in order to investigate a number of detailed aspects of the model. The predicted behaviour has been confirmed in terms of the magnitude of the response of the track and the wheel and the apparent damping of the wheel during rolling. An experimental estimate of the filtering introduced by the finite contact patch length is also possible.

1. INTRODUCTION

A theoretical model for railway rolling noise was first developed by Remington [1, 2] on the assumption that surface irregularities (usually referred to as roughness) of the wheel and/or the rail introduce a relative displacement between wheel and rail in the vertical direction. This displacement is transmitted as vibration into the wheels and rails, and it is this vibration that radiates the noise. This model was expanded substantially by Thompson [3–7] and has been implemented in the TWINS software package (Track–Wheel Interaction Noise Software), as described in reference [8].

0022–460X/99/240587 + 23 $30.00/0

Experimental validation of these respective models has been presented in references [2] and [9]. It has been shown that the noise radiation from vibrating wheels and rails with known vibration levels can be predicted reasonably accurately (see also reference [10]) but that the prediction of vibrational responses from the roughness input is subject to greater uncertainties. In particular, in reference [9], it was found that verification of the validity of this part of the model was limited by the rather large uncertainties in the roughness inputs, which were up to ± 5 dB in some one-third octave bands.

A further set of validation experiments is reported here, which were carried out in the Spring of 1990, but have not previously been published. These experiments were performed by Vibratec with the assistance of French National Railways (SNCF). Their aim was to give a more detailed validation of the part of the model which predicts the vibration generation. In order to allow accurate measurements to be made at single frequencies of excitation, sinusoidal profiles were machined onto the wheel running surface. According to the model [1, 3], when running at a speed V km/h over a sinusoidal roughness of wavelength λ m, vibration at a single excitation frequency, f Hz, of

$$f = V/3{\cdot}6\,\lambda \tag{1}$$

will be generated.

2. MEASUREMENTS

2.1. EXPERIMENTAL ARRANGEMENT

A series of three nominally similar wheelsets was selected, of the type normally fitted to an SNCF Corail passenger coach. On each of these six wheels a sinusoidal irregularity was machined, in most cases having a different wavelength. The wavelengths and intended amplitudes of the irregularities are listed in Table 1. The choice of wavelengths and the pairing of the wheels (1 with 4, 2 with 6 and 3 with 5) were such that the irregularities of the two wheels on an axle were not harmonically related. All six wheels had a diameter at the running surface of $893 \pm 0{\cdot}3$ mm.

The amplitude of the sinusoidal irregularities was chosen such that it was not large enough to cause the local curvature of the wheel surface to become concave at a trough of the irregularity. If this were to happen, the trough of the irregularity would not normally come into contact with the rail. Nevertheless, for the shortest wavelength (wheel 6) the curvature of the initial irregularity exactly cancels that of the wheel at a trough and for wheel 4 it almost does. Once they had worn (see section 2.2) this would no longer be the case.

In all cases, a section of the running surface 54 mm wide was machined, between 52 and 106 mm from the flange-back. This is wide enough to ensure that the contact patch between the wheel and the rail always occurs completely within the machined area. Apart from the sinusoidal irregularity in the longitudinal direction, the running surface was machined with a conical transverse profile inclined at 1:20 to the axial direction.

TABLE 1

Details of the sinusoidal roughness profiles used. Amplitudes are peak-peak amplitudes in μm

Wheel number		1	2	3	4	5	6
Number of waves on circumference		40	60	100	150	150	250
Wavelength (mm)		70·1	46·8	28·1	18·7	18·7	11·2
Intended amplitude		30	30	30	30	15	15
Measured amplitude at 0 km	60 mm from flangeback	29	30	19†	27	9·5†	14·5
	70 mm from flangeback	28	27	22†	29	6·5†	13·5
	80 mm from flangeback	29	29	27†	30	11†	13·5
Measured amplitude at 1000 km	60 mm from flangeback	27	29	16	22	7·5	8·5‡
	70 mm from flangeback	30	26	19	22	6	5·5‡
	80 mm from flangeback	30	28	23	27	8	10‡

† Measured at 200 km. ‡ Measured at 800 km.

Each wheelset was fitted to the test vehicle for the duration of one week, during which time four test runs of 200 km each were performed. The first two test runs were used to measure the response of one of the machined wheels, and the remaining two runs for the other wheel. Each test run followed the same route, from Juvisy, 20 km from Paris, to Les Aubrais on the main line from Paris to Bordeaux, and back. In addition, separate trackside measurements were carried out at an instrumented section of track part way between Juvisy and Les Aubrais. For each wheelset between 7 and 9 runs of the train at different speeds over the instrumented track section were recorded.

Throughout the tests the track consisted of continuously welded UIC60 rail on concrete bibloc or wooden sleepers in ballast. Only results on concrete sleepers are presented. Nabla fasteners with a 9 mm rubber pad were fitted throughout.

The roughnesses of the wheels were monitored at regular intervals during the measurement programme. Prior to the tests the natural frequencies of each of the wheels were determined using excitation by an instrumented hammer and vibration measurements with accelerometers.

2.2. ROUGHNESS MEASUREMENTS OF THE WHEELS

The roughness profile of each of the two wheels in use was measured after every 200 or 400 km. To do this, the wheelset was jacked clear of the track and rotated at a constant low speed by an electric motor. An LVDT displacement transducer was used to measure the profile. Measurements were taken on three parallel lines, at 60, 70 and 80 mm respectively from the flange-back of the wheel, the centre of this region corresponding to the nominal running line.

As an example, Figure 1 shows the measured profile of wheel 2 with a wavelength of 47 mm before and after the tests. Also shown is the spectrum of the initial profile showing the single frequency nature of the excitation it

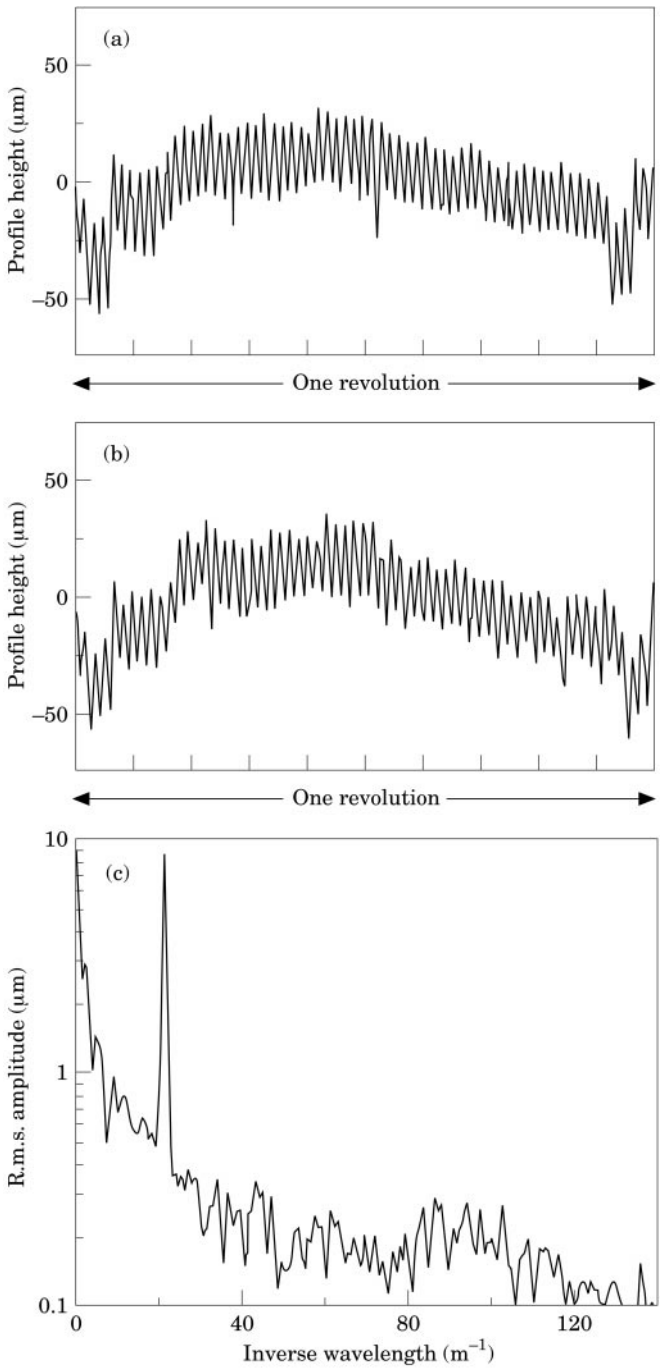

Figure 1. Roughness profile measurements on wheel 2 with wavelength 47 mm at 70 mm from the flangeback. (a) At 0 km; (b) after 1000 km; (c) spectrum of roughness after 1000 km.

provides to the wheel/rail system. In Table 1 the measured amplitudes of the sinusoidal roughnesses at the start and end of testing are also listed. The longer wavelength patterns (wheels 1 and 2) were virtually unaltered during the

1000 km of running, whilst for wheels 3 and 4 the amplitude was reduced by up to 25% and for wheels 5 and 6 the reduction was more than 50%, particularly in the centre of the measured region. However, even after 1000 km, the spectral peak corresponding to the sinusoidal component was more than 20 dB higher than the background random roughness level in all cases. The degree of wear (mostly less than 10 μm) and the low distances covered are such that the transverse profiles would not change significantly.

The only harmonic which was visible in any of the roughness spectra was the first harmonic (twice the fundamental frequency). The amplitude of this harmonic was found to be always more than 20 dB, and mostly 30 dB, lower than the fundamental component. For wheels 1–3 the first harmonic was not visible at all above the background random roughness spectrum.

2.3. ON-BOARD MEASUREMENTS

Each of the test wheelsets in turn was located under a four-axled Corail passenger vehicle. When travelling away from Paris, this was always the trailing wheelset of the leading bogie of this vehicle. The wheelsets of the trailing bogie of the previous coach (when travelling in this direction) and all other wheelsets of the test coach were reprofiled to give a smooth surface directly before the measurements, and the brakes were disabled from the test wheelset and the other wheelset in the same bogie to ensure that these wheels did not roughen due to braking action.

Three accelerometers were fitted to the test wheel, two measuring the axial acceleration of the web at different radii and one measuring the radial response of the web near the tyre. The signals from these accelerometers were passed to the recording equipment in the coach via telemetry equipment. All measurement channels were recorded simultaneously on a multiple channel tape recorder.

The measurements were performed by increasing the train speed very gradually from 30 to 160 km/h over a period of about 15 min. Moreover, around particularly critical speeds (where the wheel vibration amplitude varied rapidly), measurements were performed for some even more gradual accelerations of the train.

All the results were processed using a spectrum analyser utilising a Hanning window. In the range up to 1 kHz, a bandwidth of 1·25 Hz was used; up to 4 kHz the bandwidth was 5 Hz. The frequency range covered by each sinusoidal profile is given in Table 2. Also given is the variation in excitation frequency during the acquisition of one spectrum due to the gradual acceleration of the train. This variation is less than the bandwidth of the spectral analysis, apart from the low frequency analysis for wheels 3–5. The acquisition time of each sample is almost always long enough to include a complete wheel revolution (at 30 km/h this is 0·33 s, and at 160 km/h it is 0·063 s).

Spectra were produced using a peak-hold function on the analyser. These thus indicate the envelope of the responses to a single excitation frequency occurring at different train speeds. Examples are shown in Figure 2 in the form of vibration displacement level minus roughness level (0 dB thus corresponds to a vibration of equal amplitude to the roughness). In each case, the roughness

TABLE 2

Frequency range associated with each wheel during gradual acceleration from 30 *to* 160 *km/h. The acquisition of each spectrum takes* 0·8 *s for analysis over the frequency range* 0–1 *kHz and* 0·2 *s for* 0–4 *kHz*

Wheel	Wavelength (mm)	Frequency range (Hz)	Frequency variation (Hz) due to acceleration during 0·8 s	Frequency variation (Hz) due to acceleration during 0·2 s
1	70·1	120–630	0·6	–
2	46·8	180–950	0·9	–
3	28·1	300–1580	1·4	0·3
4,5	18·7	445–2370	2·1	0·5
6	11·2	740–3970	–	0·9

amplitude used is the average of the result on the three measurement lines, corresponding to the most recent or next measurement. Comparisons of two to five different results with each wheel revealed a high level of consistency, provided that the track type was the same. Slight differences were found when curving or when running in the opposite direction.

2.4. TRACKSIDE MEASUREMENTS

Trackside measurements were made at one track section consisting of concrete bibloc sleepers. Accelerometers were located on the rail in the vertical and lateral directions at two sections, 3·5 m apart, one above a sleeper, the other mid-way between two sleepers. An optical detector was used to locate the passing train precisely. All measurement channels were recorded simultaneously. The train passed the site at between seven and nine constant speeds for a given pair of measurement wheels. The vibration levels were analysed over a time corresponding to about 1 m of travel of the train, centred on the instant that the measurement wheel was directly over the accelerometers. This allows the response at the wheel–rail contact point to be closely approximated. The analysis time could not be made any shorter due to limits on the frequency resolution, and in any case only about one third of the wheel circumference excites the rail during this time.

The results are dominated by the excitation frequency, although at higher speeds the spectrum of the vibration contains two peaks as a result of a "Doppler shift". An example is shown in Figure 3. The higher frequency peak corresponds to waves travelling in front of the wheel, and the lower frequency peak to waves travelling in the opposite direction to the train behind the wheel. The magnitude of this Doppler effect depends on the ratio of the train speed to the wavespeed in the rail, and can therefore be expected to depend on frequency and to differ between the vertical and lateral vibration measurements. Some results will be presented in section 6.3.

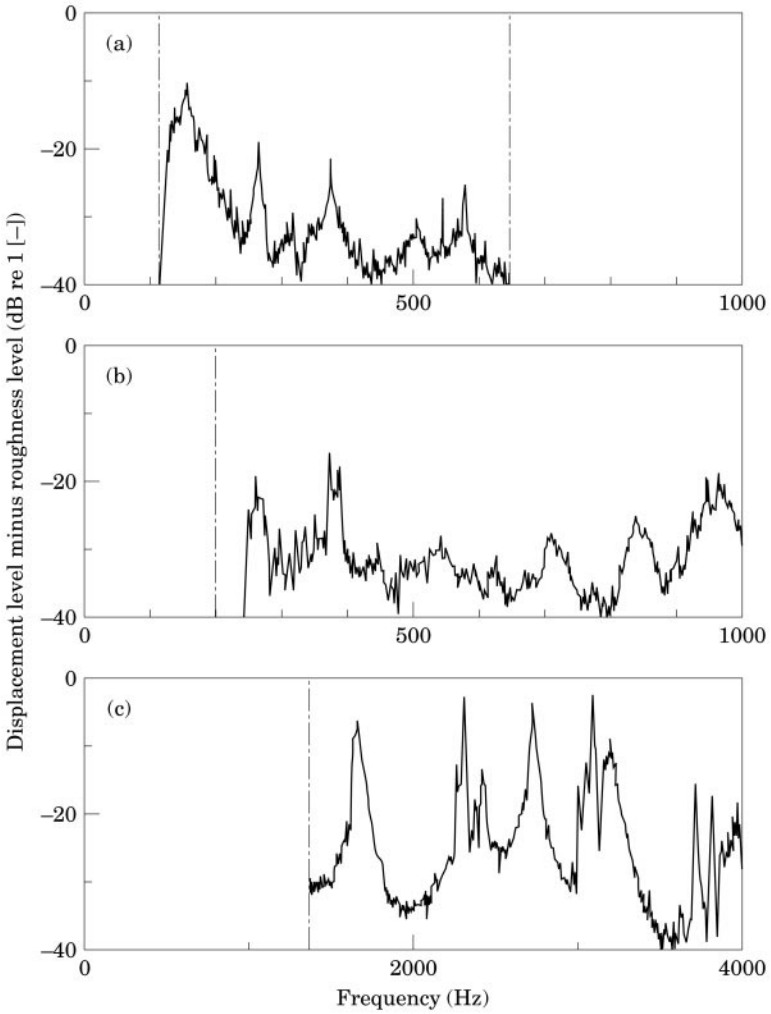

Figure 2. Measured wheel vibration level in radial direction minus roughness level. (a) wheel 1, wavelength 70 mm; (b) wheel 3, wavelength 28 mm; (c) wheel 6, wavelength 11 mm.

3. THEORETICAL MODEL

The theoretical model under investigation has been described in detail in references [3–8]. It is based on the hypothesis that an irregularity on either the wheel or the rail introduces a relative vertical displacement between the wheel and rail. This causes vibrations of the wheel and the rail, the magnitude of which depends on the relationship between their respective frequency response functions (receptances). At high frequencies the receptance corresponding to the local stiffness of the contact zone is of the same order of magnitude as the receptances of wheel and rail, and consequently some of the excitation is absorbed in the compression of the contact 'spring'.

The vibrations at the contact area are transmitted to the rest of the wheel as well as along the rail and into the sleepers. These vibrations are then responsible

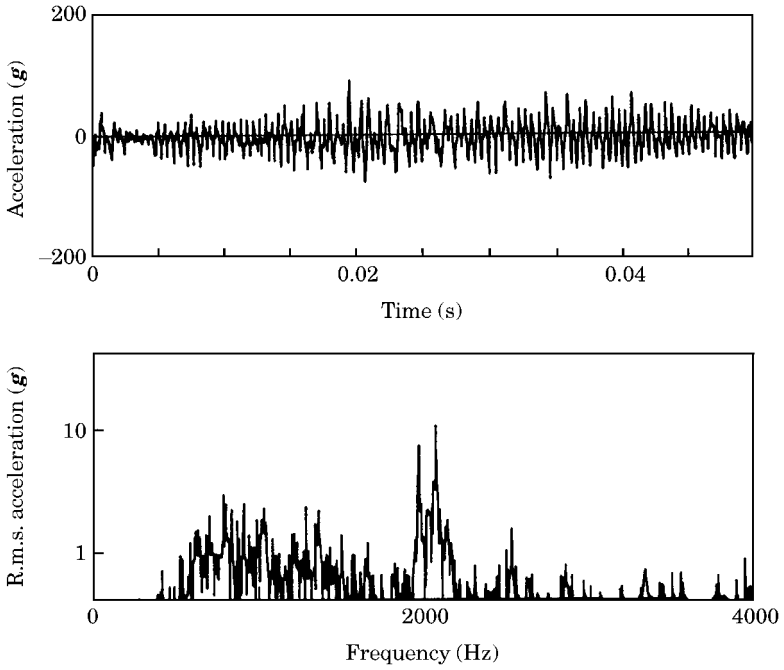

Figure 3. Measured vertical rail vibration due to the passage of wheel 4 (wavelength 18·7 mm) at 140 km/h. (a) time-dependence, with the wheel passing over the measurement point at the centre of the interval shown, (b) spectrum of this part of the signal showing split peaks.

for radiating noise. In the work described here only the generation of vibrations at the contact zone, and to a limited extent their transmission into the wheel, are considered. In any case, the other parts of the model have already been satisfactorily validated, as described in reference [9].

In order to model the wheel, a modal basis of natural frequencies, mode shapes and damping ratios is required. In order to obtain this a finite element analysis of a Corail type wheel was performed and compared with experimental results. This analysis preceded the field experiment, and was based on a worn Corail wheel with a diameter of 870 mm, which unfortunately differed from the condition of the wheels used in the field tests (diameter 893 mm). The modes of a wheel are categorised by their number of nodal diameters, $n = 0, 1, 2, \ldots$ and for axial modes also their number of nodal circles, $m = 0, 1, 2$. In addition, predominantly radial modes with different values of n occur [4]. Only the wheel was modelled, ignoring the axle by imposing a rigid boundary condition at the inner edge of the hub, as in reference [4]. This means that the modes with $n = 1$, which are normally coupled to bending of the axle, will be incorrectly predicted. To a lesser extent those with $n = 0$ will also be incorrect. However, the modes of vibration which are of most importance in the generation of rolling noise are the radial and 1-nodal-circle modes with $n \geqslant 2$ [4, 10], which will not be affected by this simplification. The natural frequencies predicted using this finite element model are compared in Table 3 with those measured in the laboratory on a free

TABLE 3

Measured and predicted natural frequencies of a Corail wheel, worn to a diameter of 870 *mm, in* Hz

No. of nodal	0 nodal circle		Radial		1 nodal circle		2 nodal circle	Circumferential
Diameters	Meas.	Pred.	Meas.	Pred.	Meas.	Pred.	Pred.	Pred.
0	302	336	3001	3167	–	1745	4778	–
1	274	246	–	1378	–	2034	4800	3454
2	389	402	1881	1961	2552	2587	5030	4594
3	998	1018	2593	2616	3166	3170	5250	–
4	1795	1817	3403	3396	3841	3834	–	–
5	2694	2707	4273	4252	4601	4570	–	–
6	3650	3640	5143	5131	–	–	–	–
7	4637	4584	–	–	–	–	–	–

wheelset. The difference between measured and predicted natural frequencies is at most 4% for modes with $n \geqslant 2$.

The natural frequencies of the wheels used in the field experiment were found to be up to 10% lower than those measured in the laboratory, because of the differences in diameter. Because the resulting difference between measured and predicted natural frequencies was rather large, the average natural frequencies measured on the wheels used in the field tests have been substituted in the modal basis which is used in the calculations. The modal damping loss factors were taken from measurements on the free wheel. Values between 1×10^{-4} and 5×10^{-4} were used for the modes with $n \geqslant 2$, higher values for the modes with $n = 0$ or $n = 1$.

For the track, several different models are available [11]. In this study the track has been represented by a model in which the rail is represented by a Timoshenko beam and the rail pads, sleepers and ballast are treated as a spring mass spring equivalent continuous support. The parameters used in this track model are listed in Table 4.

In order to determine the values of the rail pad stiffness and ballast stiffness, an impact hammer was used to measure accelerances, that is acceleration divided by force as a function of frequency. Unfortunately, it was not possible to obtain these results at the test site itself, so results from another, similar site have been used. This had a smaller rail section (UIC50 which has a mass per unit length of 50 kg/m) but importantly it had the same type of rail pads, fasteners and sleepers. In Figure 4 the measured vertical frequency response function of the track is compared with predictions. Differences can be seen between the measured accelerance above a sleeper and that between sleepers, especially around 1 kHz, the so-called pinned–pinned frequency, where a half bending wavelength fits between two sleepers. A prediction based on a continuous track model would not distinguish between these locations, so a model in which the rail is periodically supported is used to predict these accelerances. Agreement between measurement and prediction can be seen to be generally good. The rail pad stiffness determines the frequency of the broad resonance seen at around

TABLE 4

Track parameters used in the calculations

	Vertical		Lateral
Rail bending stiffness (MN m^2)	6·42		1·07
Rail mass per unit length (kg/m)		60	
Pad stiffness (MN/m)	480		100
Pad damping loss factor	0·25		0·25
Half-sleeper mass (kg)		122	
Sleeper spacing (m)		0·6	
Ballast stiffness per half sleeper (real part) (MN/m)	50		70
Ballast damping loss factor	1·0		1·0

600–700 Hz, confirming the choice of parameters listed in Table 4. The same type of rail pad was installed on the test section over which the running tests were performed.

The continuous track model, used in the remainder of this study, although not distinguishing between the accelerances at a sleeper and between sleepers, nevertheless provides an adequate estimate of the spatial average of the accelerance.

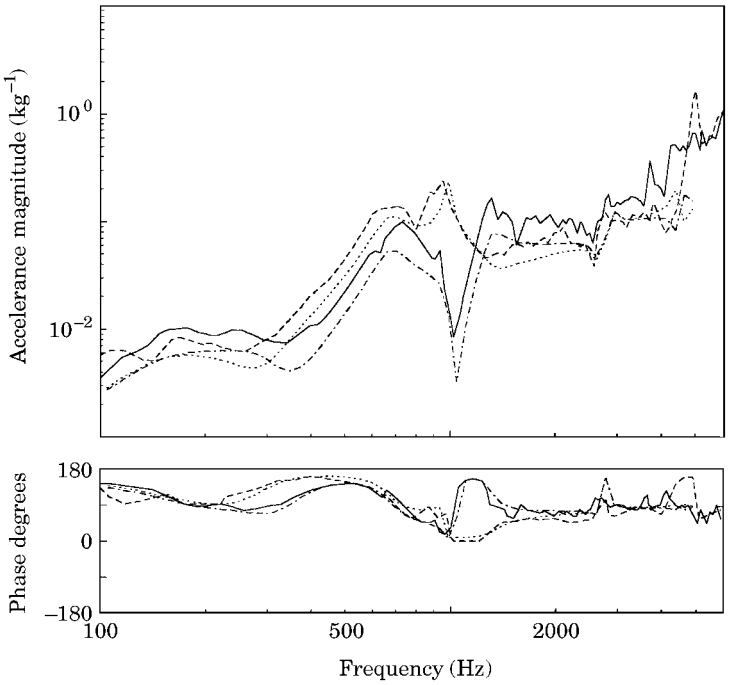

Figure 4. Predicted and measured vertical rail accelerance for a track with UIC50 rails, bibloc sleepers and similar fasteners and rail pads to those in the track used for the running tests. ———— measured above a sleeper; - - - measured between sleepers; –·– predicted above a sleeper; ····· predicted between sleepers.

4. CONTACT FILTER EFFECT

According to the model in reference [1], the wheel–rail system does not respond to very short wavelengths as well as it does to long wavelengths. This arises due to the finite length of the contact patch between the wheel and the rail. In particular, when the wavelength is short in comparison with the length of the contact patch, the excitation will be attenuated. An analytical model is given in reference [1]. The filtering effect which it predicts depends on the degree of correlation of the roughness across the width of the contact patch, according to a parameter, α. In the current situation, clearly the sinusoidal irregularities will be highly correlated across the contact patch, corresponding to a low value of α.

The rail response has been measured for certain frequency ranges using more than one wavelength of excitation (at different speeds). The response at different frequencies depends on the receptances of wheel, rail and contact spring at those frequencies as well as the roughness amplitude. By comparing the responses for different excitation wavelengths at a common frequency, the receptance effects are eliminated. Any remaining differences allow an estimate to be obtained of the contact filtering effect, which should depend on the wavelength rather than on the frequency. The contact filtering effect will also depend on the contact patch dimensions, but these should be similar for each test wheel as they have the same new transverse profiles.

The various rail responses are plotted in Figure 5 in the form of vibration displacement level minus roughness level. As in Figure 2, 0 dB corresponds to a vibration of equal amplitude to the roughness. By assuming that the longest wavelength, 70 mm, experiences no contact filtering, it can be deduced by comparing the frequency region where the results overlap, that the next two wavelengths, 47 and 28 mm, also experience negligible filtering. At the shorter wavelengths an average difference between the results in Figure 5 where they overlap in frequency can be used to deduce a filtering effect of about 6 dB on wheel 4 which has a wavelength of 18·7 mm, and 12 dB on wheel 6 with a wavelength of 11·2 mm. Wheel 5, which also has wavelength 18·7 mm, has a lower attenuation than wheel 4. These results will be compared with predictions in the next section where it will be seen that the apparently large scatter in the results for a given wheel are consistent with variations in predicted response. The estimated values of contact filter attenuation are listed in Table 5. Equivalent values have been derived from the wheel vibration and these are also given in Table 5. These are similar to those derived from the rail vibration.

These values of contact filtering, which have been implied from the measurements, can be compared with analytical results using the model from reference [1]. For this a value of α has to be selected. Figure 6 shows the analytical results for four different values of α, based on a contact patch length of 11 mm. The results derived from the measurements are also plotted. It is found that for further reductions in α below the smallest value of α shown, 0·01, the results are not significantly altered. This low value of α corresponds to a high degree of correlation across the contact, as expected for the sinusoidal roughness. These results, also listed in Table 5, agree with the measured results quite well.

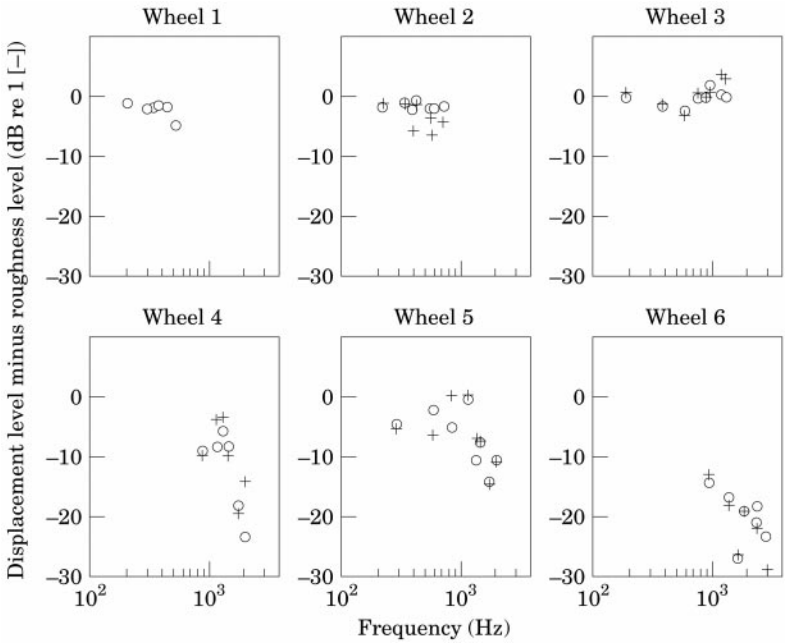

Figure 5. Measured vertical rail vibration level minus roughness level. ○: above a sleeper; +: between sleepers.

The last row of the table shows results from reference [9]. These are predictions using a numerical model of the contact zone [12] and using as input a detailed set of measured random roughness data. The results given here are the mean values from six sets of measured data, three wheels and three rails, which showed a total spread of approximately ± 4 dB in each 1/3 octave band. These latter results, in which the degree of correlation across the contact patch width is clearly less than in the current experiments, agree more closely with the analytical results for $\alpha = 5$, which are also listed in the table. However, it was found in reference [9] that at shorter wavelengths than considered here, the filtering effect was considerably less than that predicted using the model from reference [1].

TABLE 5

Average measured contact filter effect in dB, with theoretical results for comparison. The first three rows of results correspond to sinusoidal roughness, the last two to random roughness

Wavelength (mm)	70·1	46·8	28·1	18·7	18·7	11·2
Amplitude (μm)	29	28	20	26	7	12
Measured, rail	0	0	0	−6	−2	−12
Measured, wheel	0	0	0	−4	0	−12
Analytical ($\alpha = 0{\cdot}01$)	−0·3	−0·6	−1·7	−4·0	−4·0	−14·4
Analytical ($\alpha = 5$)	−2·2	−4·1	−7·4	−11·6	−11·6	−22·6
Estimated using actual random roughness [9]	−4	−4	−6	−9	−9	−14

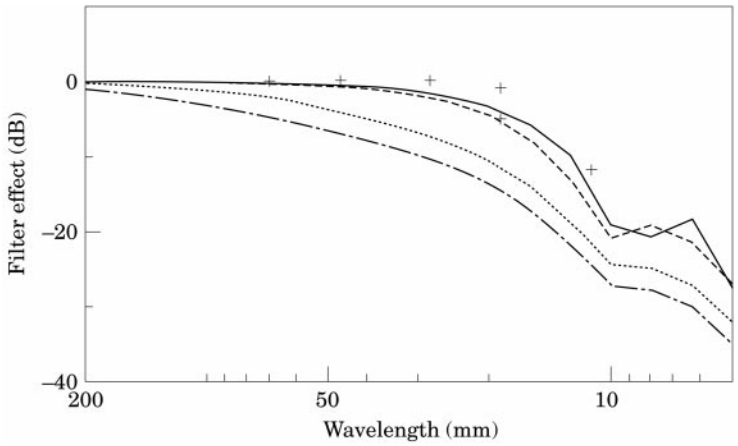

Figure 6. Contact filter effect predicted using analytical model from [1] and averaged over 1/3 octave bands. ————, $\alpha = 0{\cdot}01$; ---, $\alpha = 1$; –·–·, $\alpha = 5$; ·····, $\alpha = 10$. +: average effect derived from measurements on the wheel and the rail.

5. WHEEL RESPONSE

5.1. GENERAL FORM OF WHEEL VIBRATION RESPONSE

Comparing the measured radial wheel vibration from Figure 2 with the equivalent prediction given in Figure 7, it can be seen that similar trends are found. The predicted response at low frequencies is generally between −20 and −40 dB relative to the roughness, and rises above 0 dB at a series of peaks above 1·5 kHz. These peaks correspond to wheel resonances. In the measurements for wheels 4–6 the measured response needs to be modified to remove the contact filtering effect as discussed above, which leads to the peaks in Figure 2(c) being lower than in Figure 7. This will be considered in more detail in section 5.4 below.

The wheel response below 1 kHz is found to vary significantly between the different wheels, even after allowing for the contact filter effect. The lateral position of the contact on the wheel has a significant influence on the predicted response at low frequencies. Predictions reveal that, at these low frequencies, variations of more than 10 dB can occur for an offset of the contact position on the wheel of 15 mm. Given the level of these uncertainties, the measurements and predictions are consistent.

5.2. FREQUENCIES OF MAXIMUM RESPONSE

In the vibration spectrum of a rolling wheel, peaks occur close to the natural frequencies of the free wheel [13]. According to the theoretical model [7], the frequency of maximum response is slightly higher than the corresponding natural frequency. Table 6 lists the predicted and measured differences between the frequency of maximum response and the natural frequency. The measured values are subject to an uncertainty of ± 5 Hz. Furthermore they represent a range of values which are obtained from several of the wheels under test.

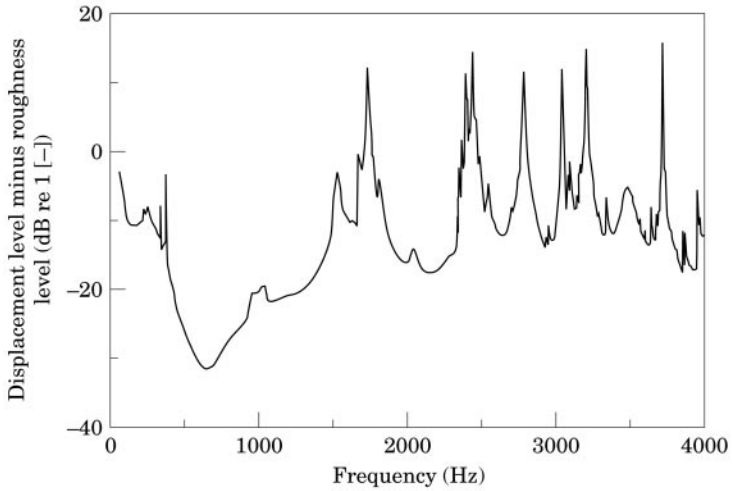

Figure 7. Predicted wheel vibration level in the radial direction at a position corresponding to the accelerometer position shown normalised to the roughness level.

The predictions and measurements can be seen to give generally similar values for these frequency differences. In particular, in each case the results are larger for the radial modes (predicted 9–18 Hz for the modes with $n \geqslant 2$, measured average 14 Hz) than for the 1-nodal-circle modes (predicted 5–6 Hz, measured average 7 Hz). The 0-nodal-diameter radial mode has in each case the largest frequency difference (about 20 Hz). These results therefore confirm this aspect of the theoretical model.

5.3. DAMPING VALUES DURING ROLLING

The apparent damping of the wheel when rolling along the track is considerably higher than the damping of a free wheel, due to the interaction with the track. This apparent damping can be estimated from the bandwidth of the peaks corresponding to the wheel resonances in both the measured and predicted responses. The bandwidth at 3, 7 or 10 dB below the peak level was used for this. The measured data for wheel 6 were used for this analysis as they covered the relevant frequency range most closely. Table 6 lists the predicted and measured loss factors for the most important modes. The predicted values are at least a factor of 10 greater than the damping of the free wheel, which is input to the calculation. In both measured and predicted values a general decrease is found in the apparent damping as frequency increases, although the measured values are on average about a factor two higher than the predicted values.

5.4. AMPLITUDE OF THE VIBRATION RESPONSE PEAKS

The measured wheel response at frequencies above 1500 Hz is dominated by the peaks corresponding to wheel resonances (see Figure 2). These measurements are only available for wheel 6. In order to compare the levels of the response at these peaks with the predictions, two corrections have to be made. Firstly, the contact filter effect for the 11 mm roughness wavelength, estimated at -12 dB,

TABLE 6

Difference between wheel natural frequencies and frequencies of maximum amplitude of the rolling vibration (in Hz*). Also listed are apparent damping loss factors during rolling. n is the number of nodal diameters*

			Frequency difference			Damping loss factor	
n	Mode	Natural frequency	Calculated 80 km/h	Calculated 160 km/h	Measured (range)	Predicted 160 km/h	Measured
2	Radial	1722	9	11	13/23	0·007	0·018
3	Radial	2426	17	13	5/14	0·004	0·006
0	Radial	2761	23	20	17/22	0·005	0·006
4	Radial	3186	12	14	3/22	0·003	–
5	Radial	4089	12	16	–	0·002	–
2	1-n-c	2387	5	6/10	−1/14	0·003	0·008
3	1-n-c	3030	7	6	2/13	0·002	–
4	1-n-c	3707	7	5	3/8	0·001	0·0025

has to be removed, i.e., 12 dB added. Secondly, it should be noted that the measured responses, which are peak-hold spectra for a sinusoidal input, will exhibit the peak at a particular frequency f for two excitation frequencies, $f \pm nf_0$ where n is the number of nodal diameters of the mode in question and f_0 is the rotation frequency of the wheel. In contrast, the prediction is based on a broad-band input as normally occurs, and the response from both excitation frequencies $f \pm nf_0$ will be superimposed. For this reason the measured responses are increased by a further 3 dB before making the comparison. For modes with $n = 0$, this last correction is not made as the peak is excited only once.

Table 7 compares the predicted and measured response levels (vibration displacement level minus roughness level in dB) at a number of the peaks. The differences between predicted and measured levels are mostly less than 3 dB, with an average of 1 dB over-prediction. This is very good when it is considered that the results are rather sensitive to discrepancies between predicted mode shapes and the mode shapes of the actual wheel, to variations in the actual position of the contact across the wheel, and to variations in track dynamics. The slight over-prediction of the peak amplitudes is probably linked to the under-estimation of the apparent damping when rolling (see section 5.3). From Table 7 it can be seen that the predictions in this form (vibration displacement level minus roughness level) are not very sensitive to train speed so it is unlikely that the variation of train speed during the measurements will cause significant differences.

6. TRACK RESPONSE

6.1. VERTICAL RESPONSE

The vertical response of the rail has been measured both above a sleeper and mid-way between sleepers, whereas the predictions correspond to an equivalent

TABLE 7

Predicted and measured wheel vibration axially at the centre of the web. Levels are given at the peaks associated with wheel resonances, expressed as displacement level minus roughness level in dB. The measured results are corrected for the contact filter effect and for the difference between random and sinusoidal excitation. n is the number of nodal diameters

n	Mode	Natural frequency	Calculated 80 km/h	Calculated 160 km/h	Measured
2	Radial	1722	15	13	10
3	Radial	2426	13	15	15
0	Radial	2761	1	1	4
4	Radial	3186	15	14	12
2	1-n-c	2387	13	13	12
3	1-n-c	3030	16	15	13
4	1-n-c	3707	18	21	18

continuous support. Because the track-side measurements correspond to discrete train speeds, they are only available for discrete frequencies. Measured and predicted vertical vibrations (in the form of displacement level minus roughness level expressed in dB) are compared in Figure 8. The effects of the contact filter (see Table 5) have been included into the measured results. Unfortunately no measured values are available for the track vibration above 3 kHz. The predicted results agree well with the measured results apart from a slight underprediction in the region of 300–500 Hz and 1–1·5 kHz.

Figure 9 compares the predicted rail vertical accelerance with that of the contact spring. It can be seen that these accelerances are similar in magnitude at 350 and 1000 Hz, which is the reason for a slight reduction in predicted rail response at these frequencies. This is followed by a progressive decrease in rail response above 1000 Hz, where the contact spring is effectively softer than the rail. The measured rail response corresponds to either a higher rail accelerance or a lower contact accelerance, i.e., higher value of contact stiffness. A change of approximately 3 dB would be sufficient to explain the differences between measured and predicted results in Figure 8. It is more likely that the rail receptance is underpredicted, than that the contact stiffness is incorrect. The use of the continuous track model is probably responsible for this discrepancy.

6.2. RAIL LATERAL VIBRATION

Figure 10 shows measured and predicted rail lateral vibration normalised to the roughness level. The lateral vibration level at the contact is mostly between 5 and 15 dB lower than the vertical vibration, as seen in both measurements and predictions. On the other hand the details of the prediction differ significantly from those of the measurements, with the predictions being too high for frequencies up to 500 Hz and too low for frequencies above this. This is a result of the strong dependence of the lateral vibration on the vertical–lateral cross accelerance, which is particularly difficult to predict or measure [11].

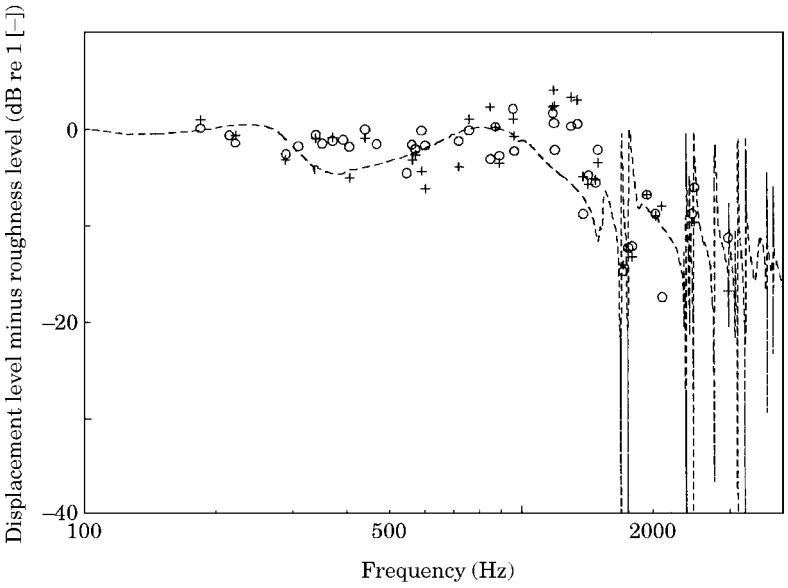

Figure 8. Predicted vertical rail vibration level minus roughness level, with measured values for comparison. ---- , predicted; ○, measured above a sleeper; +, measured between sleepers.

6.3. DOPPLER SHIFT IN THE RAIL VIBRATION

As mentioned in section 2.4, the spectrum of measured rail vibration contains two peaks at frequencies $f \pm \Delta f$, where f is the excitation frequency given by equation (1), see also Figure 3. The wave speed of vertical bending waves in the rail, c_B, can be estimated from this Doppler shift observed in the rail vibration. This is given by

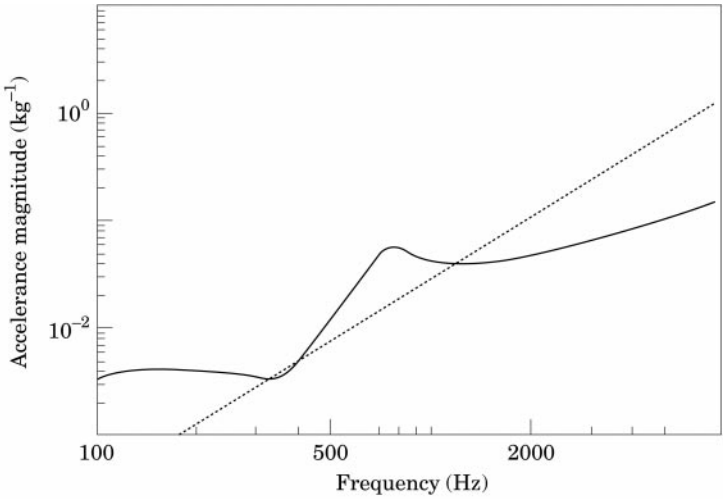

Figure 9. Vertical rail accelerance predicted using the continuous track model (————) and accelerance of the contact spring for a contact stiffness of $1{\cdot}14 \times 10^9$ N/m (----).

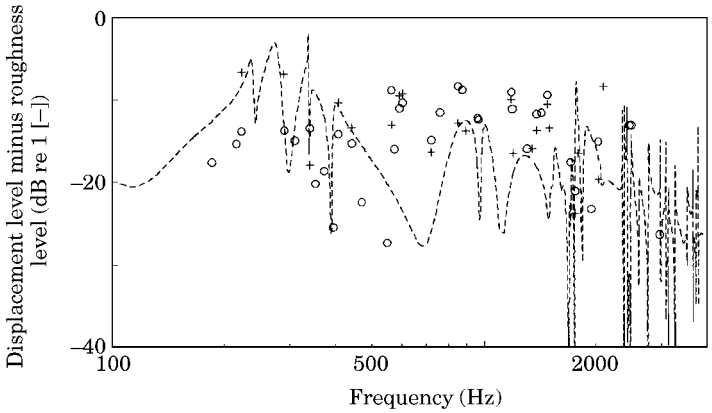

Figure 10. Predicted lateral rail vibration level minus roughness level, with measured values for comparison. ---- , predicted; ○, measured above a sleeper; +, measured between sleepers.

$$c_B = Vf/3{\cdot}6\Delta f \tag{2}$$

where V is the train speed in km/h. The separation between the two spectral peaks in the measured vibration has been converted to give an estimate of the wave speed in the rail. This has only been performed for the vertical direction. These results are plotted in Figure 11. Also shown is the predicted wavespeed as a function of frequency from the Timoshenko beam track model. Above about 1 kHz, where almost all of the measured values are found, the wavespeed is dominated by the rail. Agreement can seen to be very good in this region. At low frequencies the support stiffness and sleeper mass also play a role, but unfortunately only a single measured result could be deduced in this region as the frequency shift was mostly too small.

7. NON-LINEAR EFFECTS

7.1. INTRODUCTION

Since the theoretical models are linear, they predict that the response to a sinusoidal input is also sinusoidal. The experimental results have shown that this is predominantly the case and the results up to this point have been based on this single frequency response. However, some trace of higher harmonic response was also found, mostly only at twice the fundamental frequency. This will be quantified in this section.

It has been noted that the roughness also contains small amplitudes at the first harmonic of the intended frequency. Therefore it is important to distinguish between the response to this component of roughness and possible non-linear response to the fundamental excitation frequency.

In analysing this phenomenon, it is important to recall that the response to a given roughness amplitude is dependent on frequency. It is therefore not sufficient to compare the spectral levels at the fundamental frequency and at its

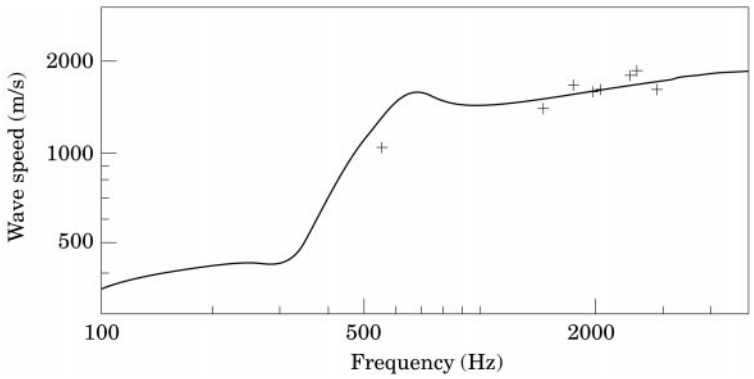

Figure 11. Predicted rail vertical bending wave speed (————), with measured values for comparison (+).

harmonics for a given running speed. Instead a comparison will be made between the response at a particular frequency when this frequency is the fundamental and when it is a harmonic of the fundamental forcing frequency. Since the frequency responses for the track are smoother than those for the wheel, the analysis is easier for the track and will be given first.

7.2. TRACK RESPONSE

For the track, an analysis has been carried out for excitation by wheels 3, 4 and 6. The response at the first harmonic is plotted in Figure 12 along with the response at the fundamental frequency. Both are normalised to the roughness amplitude at the fundamental frequency and corrected for the contact filter at the wavelength corresponding to this frequency. Comparing these responses, the average difference between the response at the first harmonic and that at the fundamental can be estimated. These are given in Table 8. For comparison, the ratio of the roughness amplitude at the first harmonic to that at the fundamental is also listed in Table 8. However, the first harmonic roughness will experience a greater contact filtering than the fundamental. From Table 5 it can be estimated that the order of magnitude of this effect is 6–8 dB, which has been added to the difference in roughness level in the last row of Table 8.

Comparing the difference in filtered roughness amplitude and the rail vibration levels it can be seen that the response at the first harmonic is not due to distortion in the roughness, which is more than 10 dB less, but is more likely a consequence of slight non-linearity in the wheel/rail system. This non-linearity is greater at short wavelengths than at longer wavelengths, but the response at the first harmonic is always less than -20 dB compared to that at the fundamental at the wavelengths considered.

In the above results, the rail vibration was normalised to the roughness amplitude at the fundamental frequency. In practice, the random roughness spectrum falls with increasing frequency, and for a doubling of frequency the roughness spectrum can fall typically 5–10 dB. This means that the non-linear component will be more apparent than stated above. Nevertheless, the linear

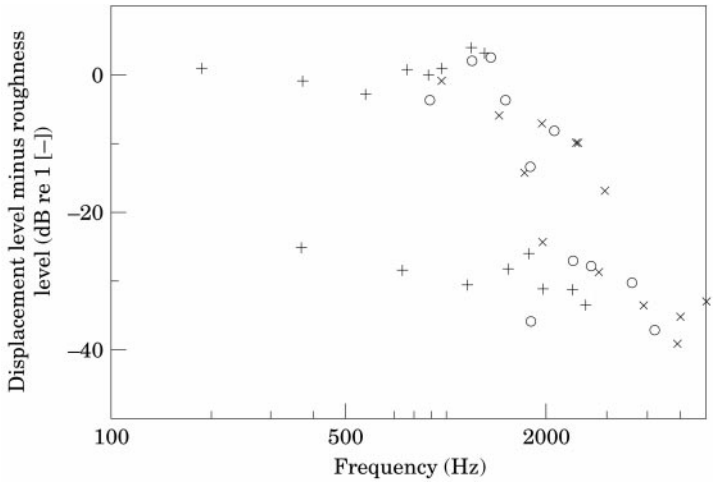

Figure 12. Vertical rail vibration at the fundamental excitation frequency (upper part of graph) and at the first harmonic (lower part of graph), normalised to the roughness amplitude at the fundamental frequency (after allowing for contact filter effect). + wheel 3, wavelength 28·1 mm; ○ wheel 4, wavelength 18·7 mm; × wheel 6, wavelength 11·2 mm.

excitation at a given frequency f due to the roughness at that frequency (wavelength $V/3{\cdot}6f$) will be at least 10–15 dB greater than the non-linear excitation due to roughness at twice this wavelength (i.e., $V/1{\cdot}8f$).

7.3. WHEEL RESPONSE

For the wheel, only the response at the peaks in the spectra above 1·6 kHz is considered as this part of the spectrum proved the most repeatable. Figure 13 shows the response of wheel 6 (wavelength 11·2 mm) tracked at the fundamental frequency and at the first and second harmonics. These are all plotted as vibration displacement relative to the fundamental roughness amplitude, with no correction for contact filtering. The ratios between the peak amplitudes for excitation at the first harmonic and at the fundamental frequency are between −15 and −25 dB. The average difference between the response at these harmonics and at the fundamental are listed in Table 9.

TABLE 8

Estimated average level difference in dB between measured rail vibration at the first harmonic and at the fundamental forcing frequency (*Figure* 12). *For comparison the difference in roughness level at these two frequencies is listed*

Wheel	3	4	6
Fundamental wavelength, mm	28·1	18·7	11·2
Difference in rail vibration level, dB	−25	−22	−20
Difference in roughness level, dB	<−30	<−26	<−24
Difference in filtered roughness level, dB	<−36	<−33	<−32

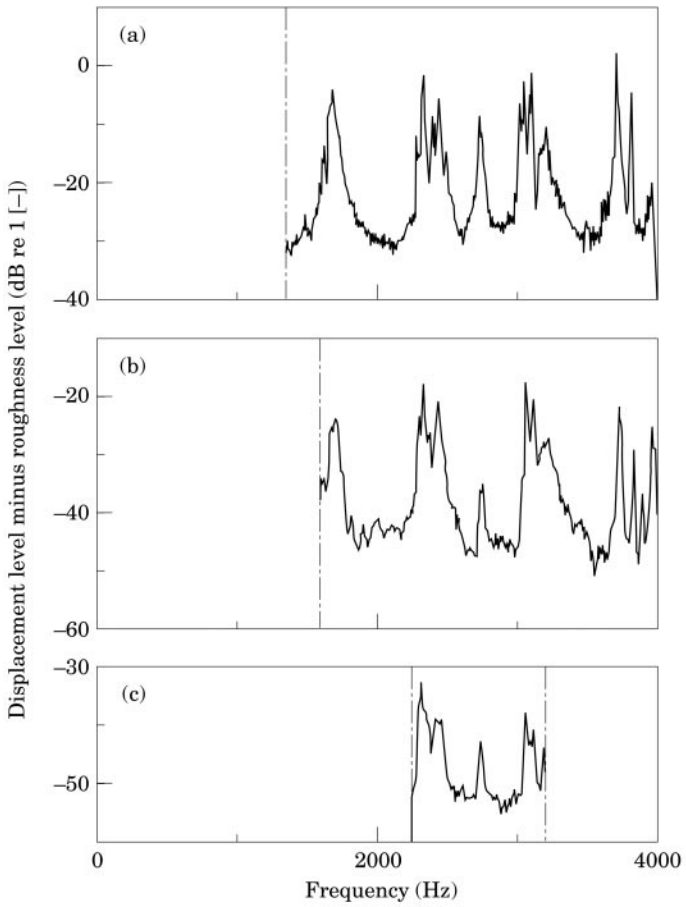

Figure 13. Axial wheel vibration on the web normalised to the roughness amplitude at the fundamental frequency. (a) response at the fundamental excitation frequency for speeds 60 to 160 km/h; (b) response at the first harmonic for speeds 30 to 80 km/h, and (c) response at the second harmonic for speeds 30 to 43 km/h.

Additional measurements were possible for wheels 4 and 5 (wavelength 18·7 mm) at a single peak at 1·7 kHz. These are given in Table 9. The ratio of the roughness amplitude at the first harmonic to that at the fundamental frequency is also listed. It can be seen that these ratios in roughness amplitude are similar to those found in the measured vibration. Taking into account the increased contact filter effect at shorter wavelength, however, it can be seen that the response at the first harmonic is higher than indicated by the roughness, but, as for the rail, is below about −20 dB. This confirms the conclusions found for the rail vibration.

8. CONCLUSIONS

A novel experiment, incorporating a sinusoidally profiled wheel, has been used to validate important components of the theoretical model for railway rolling

TABLE 9

Average level difference in dB between measured wheel vibration at the first and second harmonic and at the fundamental forcing frequency (*Figure* 13). *For comparison the difference in roughness level at these two frequencies is listed*

Wheel	4	5	6	
Fundamental wavelength, mm	18·7	18·7	11·2	
Harmonic	2*f*	2*f*	2*f*	3*f*
Difference in wheel vibration level, dB	−25	−29	−19	−34
Difference in roughness level, dB	<−26	<−24	<−24	–
Difference in filtered roughness level, dB	<−33	<−31	<−32	–

noise generation. On the whole a very satisfactory agreement has been found between the measured and predicted results.

The measurements have confirmed a number of features predicted by the model. Firstly it is confirmed that peaks in the wheel vibration response occur at frequencies up to 20 Hz above the resonance frequencies of the free wheel, the frequency difference being greater for radial modes than for 1-nodal-circle modes for the wheel under study. Secondly it is confirmed that the damping experienced by a rolling wheel is significantly greater than that of a freely suspended wheel. The predicted level of apparent damping of the wheel during rolling is approximately correct (loss factors of 2% at 1735 Hz falling to about 0·5% at 3 kHz). Thirdly the amplitude of the response at these peaks is predicted reliably. Although some variations were found, these will not be significant once averaging over 1/3 octave bands is carried out. Furthermore, the amplitude of wheel radial vibration below 1 kHz is much lower than the roughness, as predicted by the model.

Similarly, for the rail vibration close to the contact point, the measurements confirm that the vertical vibration amplitude is similar to the roughness amplitude for frequencies up to about 1 kHz, dropping slightly at higher frequencies. A slight discrepancy was found around 1 kHz which can be attributed to a slight underprediction of rail vertical accelerance in this case. Lateral rail vibration close to the contact point is between 5 and 15 dB lower than the vertical vibration. The predictions agree with this overall level but are unable to reproduce the exact features of the measured results.

It has been possible to estimate the effect of the contact filter by comparing the response at a given frequency due to different wavelengths at different speeds. The filtering effect for a sinusoidal irregularity is less than when a random roughness is present on the wheel and rail.

An investigation of the response at the first harmonic of the sinusoidal roughness has shown that this non-linear response is at least 10–15 dB lower than the linear response due to the roughness at that frequency. This confirms the validity of using the linear roughness excitation model.

ACKNOWLEDGMENTS

The measurements and analysis described here were carried out under contract for ERRI (the European Rail Research Institute) through its committee C163. The TWINS software package is the joint property of the UIC and BR Research and is administered by ERRI.

REFERENCES

1. P. J. REMINGTON 1987 *Journal of the Acoustical Society of America* **81**, 1805–1823. Wheel/rail rolling noise, I: theoretical analysis.
2. P. J. REMINGTON 1987 *Journal of the Acoustical Society of America* **81**, 1824–1832. Wheel/rail rolling noise, II: validation of the theory.
3. D. J. THOMPSON 1993 *Journal of Sound and Vibration* **161**, 387–400. Wheel–rail noise generation, part I: introduction and interaction model.
4. D. J. THOMPSON 1993 *Journal of Sound and Vibration* **161**, 401–419. Wheel–rail noise generation, part II: wheel vibration.
5. D. J. THOMPSON 1993 *Journal of Sound and Vibration* **161**, 421–446. Wheel–rail noise generation, part III: rail vibration.
6. D. J. THOMPSON 1993 *Journal of Sound and Vibration* **161**, 447–466. Wheel–rail noise generation, part IV: contact zone and results.
7. D. J. THOMPSON 1993 *Journal of Sound and Vibration* **161**, 467–482. Wheel–rail noise generation, part V: inclusion of wheel rotation.
8. D. J. THOMPSON, B. HEMSWORTH and N. VINCENT 1996 *Journal of Sound and Vibration* **193**, 123–135. Experimental validation of the TWINS prediction program for rolling noise, part 1: description of the model and method.
9. D. J. THOMPSON, P. FODIMAN and H. MAHÉ 1996 *Journal of Sound and Vibration* **193**, 137–147. Experimental validation of the TWINS prediction program for rolling noise, part 2: results.
10. D. J. THOMPSON 1988 *Journal of Sound and Vibration* **120**, 275–280. Predictions of the acoustic radiation from vibrating wheels and rails.
11. D. J. THOMPSON and N. VINCENT 1995 *Vehicle System Dynamics supplement* **24**, 86–99. Track dynamic behaviour at high frequencies. Part 1: theoretical models and laboratory measurements.
12. P. J. REMINGTON and J. WEBB 1996 *Journal of Sound and Vibration* **193**, 83–102. Estimation of wheel/rail interaction forces in the contact area due to roughness.
13. B. HEMSWORTH 1983 *Journal of Sound and Vibration* **87**, 189–194. Vibration of a rolling wheel—preliminary results.